Self-consistent calculation of the electronic structure and electron-electron interaction in self-assembled InAs-GaAs quantum dot structures

L. R. C. Fonseca* and J. L. Jimenez
Beckman Institute for Advanced Science and Technology, University of Illinois at Urbana-Champaign, Urbana, Illinois 61801

J. P. Leburton
Department of Electrical and Computer Engineering and Beckman Institute for Advanced Science and Technology, University of Illinois at Urbana-Champaign, Urbana, Illinois 61801

Richard M. Martin
Department of Physics, University of Illinois at Urbana-Champaign, Urbana, Illinois 61801
(Received 9 September 1997)

We have performed a detailed self-consistent calculation of the electronic structure and electron-electron interaction energy in pyramidal self-assembled InAs-GaAs quantum dot structures. Our model is general for three-dimensional quantum devices without simplifying assumptions on the shape of the confining potential nor fitting parameters. We have used a continuum model for the strain, from which the position-dependent effective mass and band diagram are calculated. The number of electrons in the dot is controlled by applying an external voltage to a metal gate on the top of a complete multilayer device containing a single dot. In order to determine the electron occupation number in the dot that minimizes the total energy of the system, we have adopted the concept of transition state as defined by Slater for shell filling in atoms. We have calculated the exchange and correlation terms of the many-body Hamiltonian using the local (-spin) -density approximation. By accounting for spins we have been able to determine the shell structure in the pyramid and to calculate the energy differences between the various spin configurations. We have also calculated the different contributions to the total electronic energy in the dot, i.e., the single-particle energies, the exchange-correlation energy, and the classical electrostatic electron-electron repulsion energy as a function of the gate voltage and number of electrons in the dot. Comparison with recent experimental data of Fricke *et al.* [Europhys. Lett. **36**, 197 (1996)] shows good agreement. [S0163-1829(98)02008-6]

I. INTRODUCTION

Due to their small sizes, self-assembled quantum dots offer an excellent opportunity to study the physics of highly confined few-electron systems. Furthermore, possible applications of quantum dot structures such as lasers,[1] spectral detectors,[2] and optical memories[3] have spurred a considerable interest in those systems.

Very recently, the work by Tarucha *et al.*[4] has demonstrated electronic shell structure and spin effects in lithographically defined quantum dots containing more than 40 extra electrons. That work showed that shell filling at small magnetic field follows the parallel spin ordering predicted by Hund's rule. In a different experiment using small self-assembled quantum dots containing up to six extra electrons,[5] the shell structure in the dots displayed an energy spectrum very different from the simple Coulomb blockade picture observed in metallic and mesoscopic structures. The combination of capacitance and far-infrared spectroscopy in the latter experiment has provided experimental information on level separation, as well as on the electron-electron interaction energy of the *s* and *p* states within a single InAs-GaAs quantum dot.

Previous calculations of the electronic structure of pyramidal quantum dots have either not considered the dot charging problem at all,[6,7] were limited to Coulomb interactions between different dots,[8] or have done so by using a simplified analytic model.[9] In this paper we address the electron-electron interaction within a single dot using a realistic structure with electron interactions treated within spin-density-functional theory. The structure analyzed is a complete multilayer device containing one pyramidal InAs quantum dot embedded in a GaAs matrix (Fig. 1). The number of electrons in the dot is controlled by applying voltage to a metal gate on the top of the device. Strain in the pyramid, wetting layer (the thin InAs layer from where the quantum dots arise[10]—see Fig. 1), and surrounding GaAs matrix is

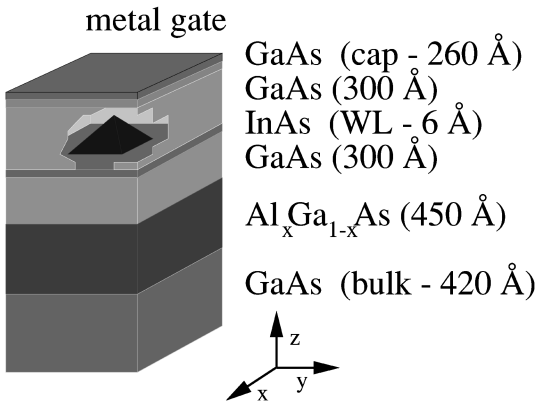

FIG. 1. Schematic representation of the self-assembled dot structure used in the present work.

calculated using a continuum model. The bulk electron effective mass and band diagram are considerably modified by the strain in the region of the dot, becoming position dependent. In order to determine accurately the bias voltage at which charging occurs, we have used the idea of transition states (Sec. II C). We have used both the local-density approximation (LDA) and the local-spin-density approximation (LSDA) to calculate the many-body interaction terms of the Hamiltonian.[11] Because LSDA provides an extra degree of freedom by considering spins, we have been able to calculate the energies of possible spin configurations in the dot showing that the dot filling indeed follows Hund's rule.

Our model has been applied to the system measured by Fricke *et al.*[5] and the numerical results compared with the experimental data. The agreement is good considering some of the approximations assumed in the calculation, and the complications involved in extracting and interpreting intrinsic properties of the dots from the experimental data.

The paper is organized as follows. In Sec. II we describe our model and the numerical techniques used. In Sec. III we discuss our results and compare them with previous calculations and experiments. Conclusions are presented in Sec. IV.

II. MODEL

A. Background

Figure 1 shows the device used in our calculation. It consists of a highly doped ($10^{18}/\mathrm{cm}^3$) 420-Å GaAs substrate, followed by a 450-Å $Al_{0.3}Ga_{0.7}As$ barrier. The active region consists of two 300-Å-wide layers of undoped GaAs surrounding a 6-Å InAs wetting layer and the InAs pyramid. A highly doped ($10^{18}/\mathrm{cm}^3$) 260-Å GaAs cap and a metallic gate complete the device. We have assumed a conduction-band offset $\Delta E_c = 770$ meV between GaAs and InAs (ratio $\Delta E_c/\Delta E_g = 70\%$), and bulk electron effective masses in GaAs and InAs of $0.067m_e$ and $0.023m_e$,[12] respectively, where m_e is the bare electron mass. As described below, those effective masses change considerably as strain is considered in the calculation (the strain calculation is indispensable for an accurate simulation of the InAs-GaAs heterostructure due to its rather large lattice mismatch, of the order of 7%). All the calculations were performed at 4.2 K.

In order to speed up the calculations, our device has been separated in two distinct regions: far from and close to the dot. In the region far from the dot we have calculated the ionized donor $N_D^+(\mathbf{r})$, ionized acceptor $N_A^-(\mathbf{r})$, electron $n(\mathbf{r})$, and hole $p(\mathbf{r})$ densities using the semiclassical Thomas-Fermi approximation for bulk charges,[13] and determined the conduction-band edge by solving the Poisson equation:

$$\nabla^2\phi = -\frac{q}{\epsilon(\mathbf{r})}[p(\mathbf{r}) - n(\mathbf{r}) + N_D^+(\mathbf{r}) - N_A^-(\mathbf{r})], \qquad (1)$$

where q is the electron charge. In the region close to the dot (defined by a box containing the pyramid, the wetting layer, and some of the GaAs surrounding matrix) we have assumed no other charges but electrons with a concentration given by

$$n(\mathbf{r}) = \sum_{i=1}^{N} n_i |\psi_i(\mathbf{r},s)|^2, \qquad (2)$$

TABLE I. Deformation potentials (Ref. 12).

Material	a_c	a_v	b
GaAs	−7.17	1.16	−1.70
InAs	−5.08	1.00	−1.80

where ψ_i is ith solution of the stationary Schrödinger Eq. (3), n_i is the occupation number of level i, N is the number of electrons, and s denotes spin. We have assumed a dot density small enough to avoid overlap between wave functions belonging to different dots and to assure the electric field can fully relax before the next dot is reached. The potential ϕ resulting from the solution of Eq. (1) is incorporated into the Schrödinger equation, written in the envelope approximation as

$$\left\{ -\frac{\hbar^2}{2}\nabla[M^{-1}\nabla] + V(\mathbf{r}) \right\} \psi_n(\mathbf{r}) = E_n \psi_n(\mathbf{r}). \qquad (3)$$

In Eq. (3), M is the electron effective-mass tensor (see below) and the potential energy V is given by

$$V(\mathbf{r}) = V_{\mathrm{ext}}(\mathbf{r}) + V_H(\mathbf{r}) + V_c(\mathbf{r}) + V_{\mathrm{xc}}(\mathbf{r}) + V_{\mathrm{off}}(\mathbf{r}), \qquad (4)$$

where $V_{\mathrm{ext}}(\mathbf{r})$ is the potential due to externally applied voltage, $V_H(\mathbf{r}) = -q\phi(\mathbf{r})$ is the Hartree potential, $V_c(\mathbf{r})$ is the conduction-band strain potential, $V_{\mathrm{xc}}(\mathbf{r})$ is the exchange-correlation potential (see Sec. II B), and $V_{\mathrm{off}}(\mathbf{r})$ is the conduction-band offset.

The strain tensor has been obtained from the minimization of the elastic energy of the system. This procedure provides the strain tensor components ϵ_{xx}, ϵ_{yy}, and ϵ_{zz}, as well as the shear components ϵ_{xy}, ϵ_{xz}, and ϵ_{yz}, which have been neglected in the present calculations.[6] The hydrostatic and biaxial components of the strain, defined as

$$\epsilon_h(\mathbf{r}) = \epsilon_{xx}(\mathbf{r}) + \epsilon_{yy}(\mathbf{r}) + \epsilon_{zz}(\mathbf{r}), \qquad (5)$$

$$\epsilon_b(\mathbf{r}) = \epsilon_{xx}(\mathbf{r}) + \epsilon_{yy}(\mathbf{r}) - 2\epsilon_{zz}(\mathbf{r}), \qquad (6)$$

respectively, play a major role in the electronic structure of the dot. Ignoring the splitoff bands, one can derive the band-edge energies at the Brillouin-zone center ($\mathbf{k}=0$):

$$V_c(\mathbf{r}) = E_g + a_c\epsilon_h(\mathbf{r}),$$

$$V_{\mathrm{hh}}(\mathbf{r}) = a_v\epsilon_h(\mathbf{r}) + \frac{b}{2}\epsilon_b(\mathbf{r}), \qquad (7)$$

$$V_{\mathrm{lh}}(\mathbf{r}) = a_v\epsilon_h(\mathbf{r}) - \frac{b}{2}\epsilon_b(\mathbf{r}),$$

where E_g is the unstrained band gap energy, and V_{hh} and V_{lh} are the heavy-hole and light-hole bands. The deformation potentials a_c, a_v, and b for InAs and GaAs are listed in Table I. Using time-independent perturbation theory up to second order, we have obtained the following expressions for the diagonal components of electron effective-mass tensor (for a detailed derivation, see Appendix A):

$$m_z^*(\mathbf{r}) = m^*(V_c(\mathbf{r}) - V_{\mathrm{lh}}(\mathbf{r}))/E_g, \qquad (8)$$

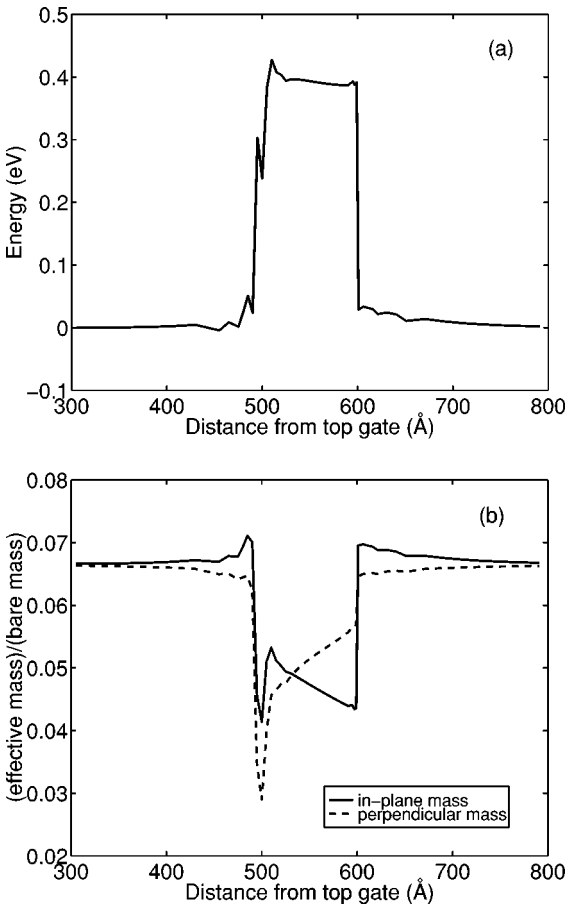

FIG. 2. (a) Strain potential; (b) perpendicular and in-plane electron effective masses along the z direction through the tip of the pyramid (in units of bare electron mass). Pyramid diameter = 200 Å and height = 100 Å.

$$m^*_{x,y}(\mathbf{r}) = m^*(V_c(\mathbf{r}) - V_{\rm hh}(\mathbf{r})) \times (V_c(\mathbf{r}) - V_{\rm lh}(\mathbf{r}))/[E_g(V_c - 0.75V_{\rm lh}(\mathbf{r}) - 0.25V_{\rm hh}(\mathbf{r}))],$$

where m^*, m^*_z, and $m^*_{x,y}$ denote bulk, perpendicular, and in-plane electron effective masses (the wetting layer lies in the xy plane). The remaining components of the effective-mass tensor are zero. It is easy to see from Eq. (8) that in the limit of small strain components $\epsilon_{xx}, \epsilon_{yy}$, and ϵ_{zz} we recover the original bulk effective mass m^*. Figures 2(a) and (b) show the strain potential and electron effective masses along the z direction, through the tip of the pyramid. Notice the large value of the strain potential and the considerable modification of the bulk effective mass, by a factor of two in average, in good agreement with the work of Cusack, Briddon, and Jaros.[6] The spikes near the tip of the pyramid are from numerical origin, caused by the difficulty in calculating the strain components around the edges of the pyramid.

The presence of the shear strains in the InAs-GaAs interfaces leads to the appearance of a polarization charge and its associated piezoelectric potential, which reduces the symmetry of the system, lifting some of the degeneracies observed in pyramidal quantum dot systems. However, piezoelectric effects in dots of the size considered in this work are very small, of the order of 1 meV as shown by Grundmann, Stier, and Bimberg[7] and our own private calculations, thus we have neglected them in this work.

Equations (8) are accurate up to second order in momentum **k**. In fact, because the confinement is so strong, the energy difference between the electron energy level and the conduction-band edge is quite large, leading to possibly large high-order corrections where nonparabolicity effects would be taken into account.[14] Such corrections would affect the position of the energy levels, which in turn set the confinement of the wave function. However, for the strongly confined states that correction would not lead to any significant change in the charge density, and therefore to the electron-electron interaction energy, which is our main investigation goal. A detailed comparison between the eight-band $\mathbf{k}\cdot\mathbf{p}$ calculation of the conduction band and the effective-mass high-order approximation is described elsewhere.[15]

Equations (1) and (3) are iterated until self-consistency is achieved. The Poisson equation is solved using the multigrid method.[16] Multigrid allows for nonuniform grids necessary to simulate relatively large devices (~ 1 μm) as the one in Fig. 1, with features as small as a few angstroms (the quantum dot and wetting layer). In addition to that, multigrid is very efficient and scales linearly with the number of grid points N_G. The Schrödinger equation is solved using the iterative extraction-orthogonalization method (IEOM).[17] The major advantage of IEOM is efficiency resulting from its ability to generate an arbitrarily small number of eigenstates N_E. As a result, the method scales as $N_E^2 N_G$, also linear in N_G.

B. Local-spin-density approximation

The usual way of calculating the exchange energy of many-electron systems in the context of device physics is to use the local-density approximation (LDA) of the Kohn-Sham density-functional theory (DFT).[18] The basic idea of DFT is to replace the rather complex N-electron wave function $\psi(\mathbf{x}_1, \mathbf{x}_2, \ldots, \mathbf{x}_N)$ and the associated Schrödinger equation by the much simpler electron density $n(\mathbf{r})$ and the corresponding functional forms $T[n]$ and $V[n]$ of the kinetic and potential energy operators, respectively. The treatment of the quantum-mechanical electron-electron interaction is left to the exchange-correlation potential $V_{\rm xc}$, which does not have an exact formulation. LDA assumes that the exchange-correlation energy $E_{\rm xc}^{\rm LDA}[n]$ can be written as

$$E_{\rm xc}^{\rm LDA}[n] = \int n(\mathbf{r})\epsilon_{\rm xc}[n(\mathbf{r})]d\mathbf{r}, \tag{9}$$

where $\epsilon_{\rm xc}[n]$ is the exchange and correlation energy per particle of a uniform electron gas of density n. The functional $\epsilon_{\rm xc}[n]$ can be separated into exchange and correlation contributions,

$$\epsilon_{\rm xc}[n] = \epsilon_x[n] + \epsilon_c[n]. \tag{10}$$

The exchange part is well known,[19] and is given by

$$\epsilon_x[n] = -\frac{3}{4}\left(\frac{3}{\pi}n(\mathbf{r})\right)^{1/3}, \tag{11}$$

in atomic units, while accurate values of the correlation part $\epsilon_c[n]$ have been obtained from quantum Monte Carlo calculations[20] as parametrized by Perdew and Zunger.[21] From Eq. (9) we can derive the exchange-correlation potential:

$$V_{\mathrm{xc}}^{\mathrm{LDA}}(\mathbf{r})=\frac{\delta E_{\mathrm{xc}}^{\mathrm{LDA}}}{\delta n(\mathbf{r})}. \tag{12}$$

LSDA offers a more general approximation for the exchange-correlation potential. In this case the exchange-correlation energy $E_{\mathrm{xc}}[n^{\alpha},n^{\beta}]$ is a function of the α-electron and β-electron densities $n^{\alpha}(\mathbf{r})$ and $n^{\beta}(\mathbf{r})$, where α and β denote spins up and down. The exchange term becomes not only a function of the total charge density $n=n_{\uparrow}+n_{\downarrow}$ but also a function of the polarization parameter ζ,[18]

$$\epsilon_x[n,\zeta]=-\frac{3}{4}\left(\frac{3}{\pi}n(\mathbf{r})\right)^{1/3}(2^{1/3}-1)f(\zeta), \tag{13}$$

where

$$f(\zeta)=\frac{1}{2}\,\frac{(1+\zeta)^{4/3}+(1-\zeta)^{4/3}-2}{2^{1/3}-1}, \tag{14}$$

and

$$\zeta=\frac{n^{\uparrow}-n^{\downarrow}}{n}. \tag{15}$$

The correlation term is calculated using the same parametrization of LDA but interpolating between the results of a spin-polarized and unpolarized free electron gas[11] depending on the spin polarization in the dot ζ. Not only is this formulation necessary for the solution of problems involving magnetic field, it usually is a better description of the real system than the LDA approximation even in the absence of magnetic field.[22] This is certainly the case in spin-polarized systems that should occur at least for an odd number of electrons in the dot.[23]

The validity of LDA and LSDA is, in principle, limited to smooth potentials, which is not the case in quantum dots since the high confinement creates electronic potentials varying in the scale of angstrons. However, the potentials created in atoms are not smooth either, and still the local approximations provide good results.[18,22] Exact calculations of the electronic structure of pyramidal dots using quantum Monte Carlo have confirmed our expectations that the local approximations indeed provide reliable exchange-correlation energies for this system, within the single-band model. A detailed comparison of the two methods is described elsewhere.[24]

C. Transition state

The desired key quantities are the energies to add electrons to the dot. If the dot is well isolated from the electrical contacts as well as from the 2D electron gas surrounding it, then it is appropriate to consider the number of electrons in the dot as integers and the change in the occupation as transitions between integer occupations. This is a valid approach if the barriers are high enough so that the overlap between the dot wave functions and the contact or the 2D electron gas wave functions is negligible. Thus we will proceed by constructing an approach for calculating the transition energies between integer occupations. Note that in the opposite limit, where the coupling to the contacts is strong, it would be more appropriate to use the fractional occupation approach with a Fermi function commonly employed in other studies.[17,25]

According to the density-functional theory, the Kohn-Sham Eq. (3) can only provide the ground state of the system and its total energy E_T. Thus, a rigorous way of determining the number N of electrons in a quantum dot with the electron charge as a good quantum number is to minimize $E_T(N)$, for $N=1,2,\ldots,N_{\max}$. This minimization should be repeated whenever the external voltage bias V_g is changed. The use of just eigenvalues to determine the charge in the dot, where charging occurs whenever an eigenvalue crosses the Fermi level, is only correct in the limit of weakly interacting electron systems.

There are two problems with the use of the total energy to determine the number of electrons in the dot as a function of bias voltage: accuracy and efficiency. The calculation of the total energy of the system involves terms of the order of meV's like the Hartree and exchange-correlation energies, and terms of the order of tens of eV's, like the electrostatic energy of the doping impurities and surface charges. The total energy of the system is of the order of tens of meV's, since the large terms mostly cancel out. Clearly such an accurate cancellation is difficult to obtain. The efficiency problem is less severe. In principle, one would have to calculate at least $E_T(N)$ and $E_T(N+1)$ for each value of V_g in order to determine if there are N or $N+1$ electrons in the dot. Since each self-consistent calculation is a time consuming operation, such a scheme should be computationally costly. The transition state concept offers an elegant solution to these problems.[26,27]

The Kohn-Sham theory is not restricted to integer numbers of electrons in the system. Differentiating E_T with respect to the noninteger occupation number n_i of level i one obtains

$$\frac{\partial E_T}{\partial n_i}=\epsilon_i. \tag{16}$$

Equation (16), called the Janak theorem,[28] provides a meaning to the eigenvalues of the Kohn-Sham equation. Integrating Eq. (16) between N and $N+1$ one finds the so-called Slater formula:[26]

$$E_T(N+1)-E_T(N)=\int_0^1 \epsilon_{\mathrm{LAO}}(n)\,dn\approx\epsilon_{\mathrm{LAO}}(\tfrac{1}{2}), \tag{17}$$

where ϵ_{LAO} corresponds the eigenvalue of the lowest available orbital. The last step in Eq. (17) is exact if ϵ_{LAO} is a linear function of the occupation number. We have performed several numerical experiments which demonstrated a nearly linear relation, showing that the approximation used in Eq. (17) is very good.

If one wishes to find out if there are N or $N+1$ electrons in the dot, one defines the transition state as the state containing $N+0.5$ electrons. Its usefulness is obvious: if $\epsilon(\frac{1}{2})$ is positive then $E_T(N+1)>E_T(N)$ and the dot contains N

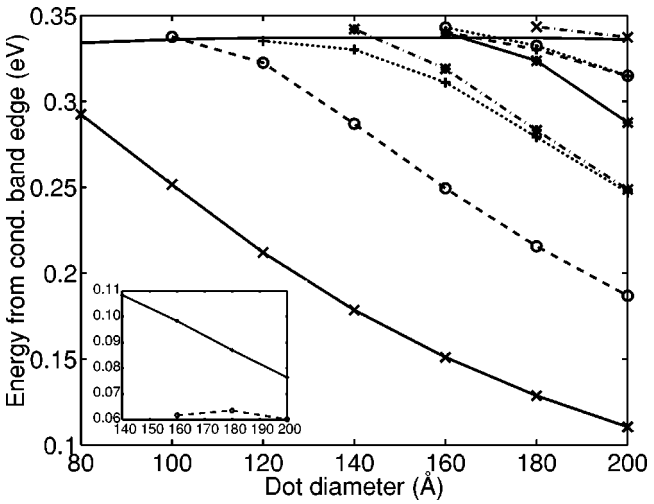

FIG. 3. Approximate well depth (thick solid line) and eigenvalues of the Hamiltonian as a function of dot diameter d. The eigenvalues were calculated with respect to the average conduction-band edge in the region of the pyramid. States represented, from low to high energy: (0 0 0), (1 0 0)/(0 1 0), (0 0 1), (1 1 0), (2 0 0)-(0 2 0), (2 0 0)+(0 2 0), (1 0 1)/(0 1 1), and (1 1 1). The notation $(n_1 n_2 n_3)$ denotes the number of wave-function nodes in the x, y, and z directions. Degenerate states are separated by a slash. Inset: energy separation between states (0 0 0) and (1 0 0)/(0 1 0) (solid), and between states (1 0 0)/(0 1 0) and (0 0 1) (dashed). Pyramid height $h=d/2$. Lines are only guides for the eye.

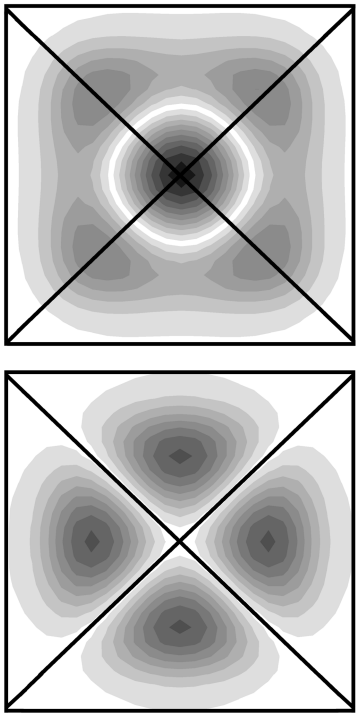

FIG. 4. Projections of the states (2 0 0)-(0 2 0) (top) and (2 0 0)+(0 2 0) (bottom). Notice the lobes of the top state along the diagonals (crossed lines) of the base of the pyramid (square box), lowering its energy with respect to the more confined bottom state.

electrons, otherwise it contains $N+1$ electrons. This procedure not only saves computer time by only solving the equations for $N+0.5$ instead of N and $N+1$ electrons in the dot, but it also circumvents the difficult problem of accurately calculating the total energy E_T of such a complex system containing dopants and metal gates. This approach for DFT where the total energy of the system is minimized keeping a fixed parameter (the charge in the dot) is called constrained DFT.[29,30]

III. RESULTS

A. Variable dot size

Figure 3 shows the first ten eigenvalues of empty dots as a function of dot base length (also called base diameter), keeping the wetting layer width fixed. The eigenvalues were calculated with respect to the average conduction-band edge position in the dot. Figure 3 and inset also show the approximate depth of the well and the energy difference between the first (0 0 0) and second (1 0 0) states, and between the second and third (0 0 1) states. The notation $(n_i n_j n_k)$ corresponds to the number of nodes of the eigenfunction in the x, y, and z directions, respectively. The eigenvalues were only calculated while the states remained bound or quasibound. Notice in the inset that the energy separation between (0 0 0) and (1 0 0) is close to linear, while between (1 0 0) and (0 0 1) it is almost a constant, reflecting the different confinement directions of the last two states. As the eigenvalues approach the top of the well, the slopes of the curves tend to decrease, as a result of deeper wave-function penetration in the barrier region. For energies above the well height, the corresponding eigenfunctions spread over the wetting layer, becoming a two-dimensional electron gas.

The Hamiltonian of this problem is invariant under the symmetry operations of the group C_{4v},[31] which allows the wave functions to be symmetrized according to the irreducible representations of this group. It can be easily checked that only p-like states [like (1 0 0)] can be degenerate, while all other degeneracies are accidental. That explains why the states (2 0 0) and (0 2 0) are not degenerate in a finite barrier pyramid, even though they are degenerate in an infinite square well. In the latter case degeneracy occurs because the Hamiltonian allows separation of variables. One can also show that the irreducible representation of those two states are the linear combinations (2 0 0)-(0 2 0) and (2 0 0)+(0 2 0), shown as the fifth and sixth curves from bottom to top of Fig. 3 (solid line with stars and dashed line with crosses, respectively). Perhaps this counterintuitive result can be more easily understood with the help of Fig. 4. It shows that the projections of the states (2 0 0)-(0 2 0) and (2 0 0)+(0 2 0) are very different, and thus are affected differently by the pyramidal confining potential. As a result, the energies of the two states do not need to be the same.

Our calculations agree well with those of Ref. 8 in the range of sizes investigated in that work. As discussed in Sec. II, these eigenvalues may change considerably if a full eight-band $\mathbf{k}\cdot\mathbf{p}$ calculation is performed.

B. Charging effects

Several measurements[5,32] as well as calculations[8,9] have addressed the problems of electron charging energy in an ensemble of pyramidal dots and the electron-electron interaction energy in a single pyramidal quantum dot. In the first case, calculations are only meaningful if several dots are

considered, as discussed in Ref. 10, since this is an effect that involves the whole ensemble of dots. The bias value at which the next electron occupies a particular dot depends on the state of the neighboring dots, whether they are occupied or not. However, because the distance between two electrons in a dot is at least one order of magnitude smaller than the distance between electrons in separate dots, the electron-electron interaction energy in a single dot is only marginally affected by the state of the other dots for typical densities of 10^{10} dots/cm^2. Besides, if one of the gates lies nearby, which is the case in some experimental setups,[5] image charges screen even further the perturbation caused by neighboring dots. Since the electron-electron interaction energy has only been indirectly inferred from experimental data and fit to calculations, we have calculated its value self-consistently using different methods for treating the electron-electron interaction and for different dot sizes.

The exchange-correlation $E_{\rm xc}$ and Hartree E_H energies are defined as

$$E_{\rm xc}[n]=\int n(\mathbf{r})\,\epsilon_{\rm xc}(\mathbf{r})\,d\mathbf{r}, \tag{18}$$

where $\epsilon_{\rm xc}(\mathbf{r})$ is the exchange and correlation energy per particle of a uniform electron gas of density n, and

$$E_H=\frac{1}{2}\int \frac{n(\mathbf{r})n(\mathbf{r}')}{4\pi\overline{\epsilon}|\mathbf{r}-\mathbf{r}'|}\,d\mathbf{r}d\mathbf{r}', \tag{19}$$

where $\overline{\epsilon}$ is the average dielectric constant, independent of position, which probably introduces only a small error to the value of E_H since the dielectric constants throughout the layers differ by less than 15%. Because direct solution of Eq. (19) is too time consuming, we have calculated the potential created only by the electrons in the dot V_e and then solved

$$E_H=\frac{1}{2}\,\frac{1}{4\pi\overline{\epsilon}}\int V_e(\mathbf{r})n(\mathbf{r})\,d\mathbf{r}. \tag{20}$$

The potential V_e is obtained by solving the Poisson equation with the density determined by the dot electrons and boundary condition calculated by multipole expansion (up to quadrupole) of the charge in the dot. This is a good approximation if the boundaries are far from the charge, which is the case in our device. However, the expansion is complicated by the presence of materials of different dielectric constants. Again, we have simplified that by assuming an uniform medium with a dielectric constant averaged over all the points of the device.

The integrations in Eqs. (18) and (20) are over the dot regions only, thus only the energy of the electrons in the dot has been taken into account. The electron-electron interaction energy $E_{\rm ee}$ is the sum of the exchange-correlation and Hartree energies.

Figure 5 shows the charging of three quantum dots of different sizes as a function of bias in the metal gate on the top of the device (see Fig. 1). In all three staircases LSDA was used to treat the electron-electron interactions. The dots were charged up to the maximum number of electrons they can fit. As expected, the step size becomes longer as the dot size decreases as a result of the more widely spaced single-

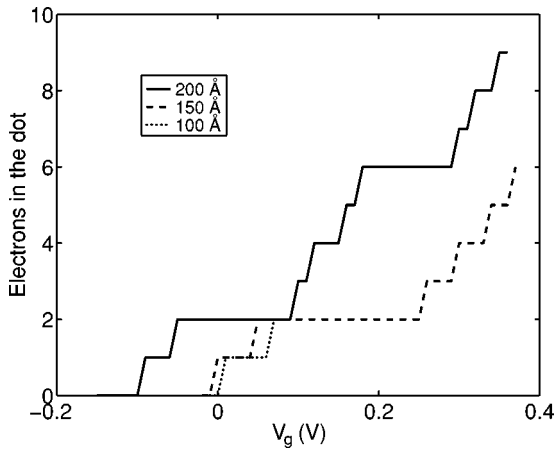

FIG. 5. Number of electrons in the dot as a function of applied voltage V_g for different pyramid diameters d. Pyramid height $h=d/2$.

particle levels (steps corresponding to $N=2$, 6, and 9, where N is the number of electrons in the dot) and the stronger electron-electron repulsion. However, the steps involving charging of degenerate levels ($N=3$, 4, and 5) become more homogeneous for smaller dots. That results from the different dependencies of the Hartree and exchange-correlation energies on the charge density, thus in the dot volume. While the first increases as n^2, the second increases only as $n^{4/3}$, as described in Eqs. (18) and (19). Thus the Hartree term, which only depends on the charge in the dot and not on the spin configuration, dominates for smaller dot sizes. The uneven steps observed for $N=3$, 4, and 5 in the 200-Å base diameter pyramid can be understood as follows. We have occupied the second (1 0 0)/(0 1 0) degenerate levels following Hund's rule, i.e., according to the spin sequence $2p_x^{\uparrow}2p_y^{\uparrow}2p_x^{\downarrow}2p_y^{\downarrow}$, where the arrows pointing up and down correspond to spin orientation and the notation $2p_i$ means the second level of type p oriented along direction i. In the next section we will show that this system indeed follows Hund's rule. The step corresponding to $N=3$ is short because the third and fourth electrons occupy different orbitals (1 0 0) and (0 1 0). Even though the two electrons have the same spin, those orbitals have a node near the center of the pyramid, resulting in small wave-function overlap. The step corresponding to $N=4$ is long because the fifth electron is forced to share an orbital already half-occupied. There is strong wave function overlap and no exchange energy, since the fifth electron spin is different from the third and fourth electron spins. Finally, the step corresponding to $N=5$ is short because, even though the sixth electron is repelled by the other three electrons, exchange between the sixth and the fifth electrons decreases the repulsion energy.

The energy of the electrons in the dot can be decomposed in single-particle and electron-electron interaction energy. The single-particle energies for empty dots are displayed in Fig. 3. As the dot is charged those energies shift up, but the energy separation between them stays approximately the same. It is interesting to compare those separations with the electron-electron interaction energy. Table II shows the variation of $E_{\rm xc}$, E_H, and $E_{\rm ee}$ using the LDA and LSDA approximations as functions of dot diameter and number of electrons in the dot. In a crude order of magnitude compari-

TABLE II. Exchange-correlation energy E_{xc}, Hartree energy E_H, and electron-electron interaction energy E_{ee} as a function of dot diameter d and occupation number N. The energies are the averages over gate voltages for each occupation number. Energies in eV, dot diameter in angstroms. Dot height $h=d/2$.

		LDA			LSDA		
d	N	E_{xc}	E_H	E_{ee}	E_{xc}	E_H	E_{ee}
	1	−0.007	0.007	0.000	−0.009	0.007	−0.002
	2	−0.018	0.027	0.009	−0.018	0.029	0.011
	3	−0.028	0.053	0.025	−0.029	0.054	0.025
	4	−0.040	0.086	0.046	−0.042	0.088	0.046
200	5	−0.052	0.129	0.077	−0.053	0.131	0.078
	6	−0.065	0.179	0.114	−0.066	0.182	0.116
	7	−0.078	0.226	0.148	−0.079	0.234	0.155
	8	−0.092	0.283	0.191	−0.093	0.287	0.194
	9	−0.105	0.351	0.246	−0.105	0.352	0.247
	1	−0.008	0.008	0.000	−0.010	0.009	−0.001
	2	−0.021	0.034	0.013	−0.021	0.034	0.013
150	3	−0.032	0.062	0.030	−0.033	0.063	0.030
	4	−0.044	0.100	0.056	−0.046	0.100	0.054
	5	−0.057	0.145	0.088	−0.058	0.147	0.089
	6	−0.070	0.198	0.128	−0.071	0.200	0.129
100	1	−0.010	0.010	0.000	−0.011	0.010	−0.001
	2	−0.023	0.039	0.016	−0.023	0.038	0.017

son, we see from Fig. 3 that the single-particle energy separation for the first two levels is of the order of 50–100 meV, while Table II shows that the electron-electron interaction energy is of the order of 10–30 meV per pair of particles, on average. Because charging of the dot involves the electronic configuration of the entire device and not only of a single dot, Fig. 5 cannot be directly obtained from Table II, which only shows electronic energies in the dot.

The electron-electron interaction energy has been calculated using both LDA and LSDA. Even though there are differences between the results of the two methods in Table II, both provide the same qualitative description of the many-body effects. Notice that E_{xc}^{LSDA} is always more attractive or at least equal to E_{xc}^{LDA}. Consequently, we have an increased density with LSDA and therefore $E_H^{LSDA} \geqslant E_H^{LDA}$. Also notice that LDA provides a better cancellation between E_{xc} and E_H for one electron in the dot. This is an unexpected result since LSDA is a better description of the physical system. One possible explanation for that is the approximate expression we have used for the Hartree energy calculation, as already discussed.

Figure 6 shows the relative difference between the LDA and LSDA calculations as a function of the number of electrons N in the dot and for two dot sizes. A striking feature is the increase of the relative difference when there are unpaired electrons in the dot, which happens for $N=1,3,4,5,7$. For $N=4$ there are two unpaired electrons, one in each of the degenerate (1 0 0) and (0 1 0) levels, leading to a high relative difference. For $N=5$ the number of unpaired electrons decreases to 1, which coincides with a decrease in the relative difference. This trend is not observed from $N=7$ (one unpaired electron) to $N=8$ (no unpaired electron) electrons in the dot, but since the relative difference for those values of N is below 1%, numerical inaccuracy may be affecting those results. As we have pointed before, LSDA is supposed to be a better approximation to the many-body exchange energy than LDA specially when there are unpaired electrons in the system giving rise to nonzero total spin momentum.

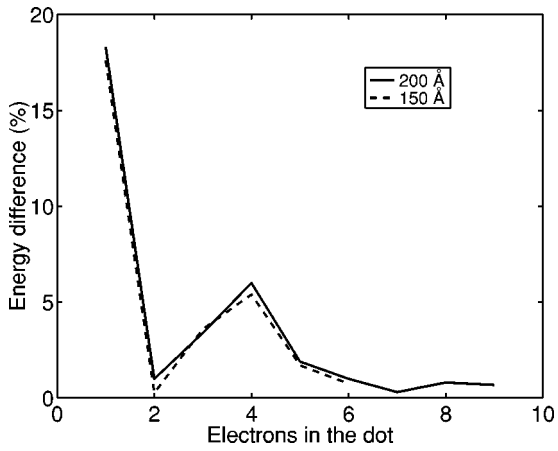

FIG. 6. Relative exchange-correlation energy difference between LDA and LSDA calculations as a function of occupation number and for different dot diameters d. Pyramid height $h=d/2$.

We now analyze the LSDA results only. The conclusions are the same for LDA since the differences between the two methods are not qualitative. In Fig. 7 we have plotted E_{xc} and E_H as a function of occupation number for the three dot sizes in a log-log scale. As expected, the Hartree energy increases approximately as n^2, faster than the exchange-correlation energy, which increases (in absolute value) approximately as $n^{4/3}$. The observed slopes are smaller than 2 and 4/3, which we attribute to wave-function penetration in the barrier at higher occupation numbers. Figure 8 shows the electron-electron interaction energy E_{ee} as a function of occupation number and for different dot sizes. This energy results from the interactions among all the electrons in the dot.

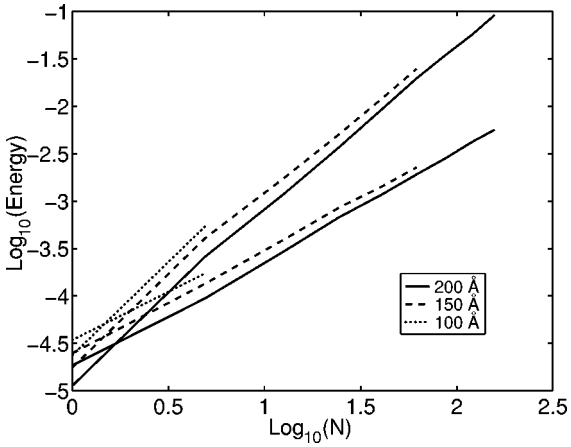

FIG. 7. Exchange-correlation energy (solid, dashed, and dotted lines of smallest slopes) and Hartree energy (larger slopes) as a function of occupation number for different dot diameters d. Offsets within each set of curves are due to different dot volumes. Pyramid height $h=d/2$.

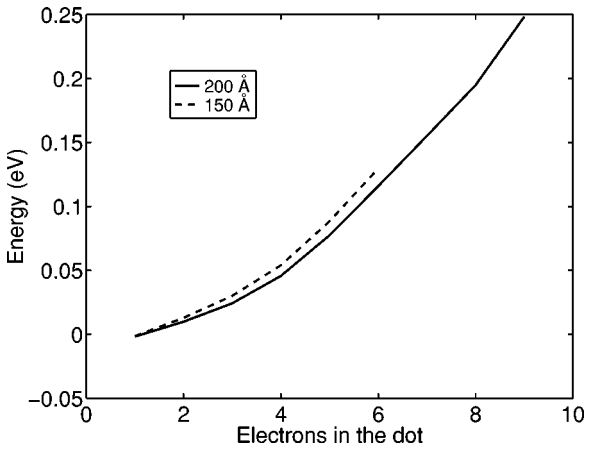

FIG. 8. Electron-electron interaction energy as a function of occupation number for different dot diameters d. Pyramid height $h=d/2$.

In the next section we will consider electron-pair interactions and compare with corresponding energies inferred from experimental data.

C. Comparison with experiment

In order to compare our results with those of Fricke *et al.* we have calculated the electronic structure of a 200 Å base diameter and 70 Å height pyramidal quantum dot. Figure 9 shows the number of electrons in such a pyramid as a function of gate voltage V_g. Three curves are shown, corresponding spin-dependent (LSDA) charging sequences that follow or do not follow Hund's rule, and a spin-independent (LDA) charging sequence. As already pointed, Hund's rule means that the charging of the fourfold degenerate second level follows the spin sequence $2p_x^{\uparrow}2p_y^{\uparrow}2p_x^{\downarrow}2p_y^{\downarrow}$. The curve that does not follow Hund's rule was obtained by charging the second level according to the spin sequence $2p_x^{\uparrow}2p_y^{\downarrow}2p_x^{\uparrow}2p_y^{\downarrow}$. The third possibility, namely, the spin sequence $2p_x^{\uparrow}2p_x^{\downarrow}2p_y^{\uparrow}2p_y^{\downarrow}$, was not considered because it will clearly be unfavorable due to the intense Coulomb repulsion between the $2p_x^{\uparrow}$ and the $2p_x^{\downarrow}$ electrons resulting from their large wave-function overlap. The step size obtained with LSDA corresponding to the charging of the fourth electron ($N=3$) is longer for the charging the dot according to the spin sequence $1s^{\uparrow}1s^{\downarrow}2p_x^{\uparrow}2p_y^{\downarrow}$ than for $1s^{\uparrow}1s^{\downarrow}2p_x^{\uparrow}2p_y^{\uparrow}$, indicating that, indeed, Hund's rule is followed by this system. The electron-electron interaction energy difference between the two spin configurations for four electrons in the dot is ~ 3 meV.

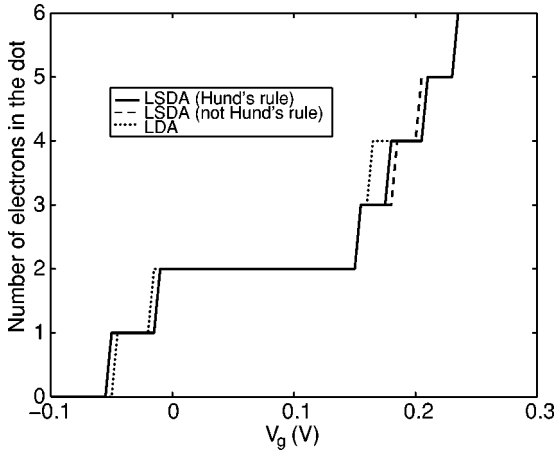

FIG. 9. Number of electrons in the dot as a function of gate voltage V_g using LSDA according to Hund's rule (second-level population following the spin sequence $2p_x^{\uparrow}2p_y^{\uparrow}2p_x^{\downarrow}2p_y^{\downarrow}$), LSDA not following Hund's rule (second-level spin sequence $2p_x^{\uparrow}2p_y^{\downarrow}2p_x^{\uparrow}2p_y^{\downarrow}$), and LDA. The dotted curve coincides with the solid curve whenever the dots are not visible. Pyramid diameter = 200 Å and height = 70 Å.

The addition of the fourth electron following Hund's rule is less costly because of the presence of exchange interaction (attractive) in this case but not if the spin of the fourth electron is different from the spin of the third. Analogously, the step corresponding to the charging of the fifth electron ($N=4$) is shorter for the sequence $2p_x^{\uparrow}2p_y^{\downarrow}2p_x^{\uparrow}2p_y^{\downarrow}$ because the fifth electron, either in the $2p_x^{\uparrow}$ or $2p_y^{\downarrow}$ state, interacts by exchange with one of the two electrons already in the second level, while according to Hund's rule, the fifth electron does not interact by exchange with any of the other two because of their different spin states.

The staircase obtained with LDA does not match either one of the LSDA staircases at some charging bias points. In the analysis of Table II it was pointed out that LSDA usually provides higher electron-electron charging energies than LDA, with an exception made for a single electron in the dot (see columns 5 and 8 of Table II). This exception can be used to explain the difference between the two LDA/LSDA curves in Fig. 9 for the charging of the first electron, while for the second electron the charging delay of LSDA follows the usual pattern. Notice, however, that Table II can only be used as a guide in the present analysis since none of the structures used for the obtention of Table II have the same dimensions as the one we now describe. The coincidence between the LDA and LSDA charging bias for the third, fifth, and sixth electrons in the dot may result from the finite voltage step size used, which also explains the finite slopes of the charging steps. The considerably large difference between the LDA/LSDA charging bias for the fourth electron results from the rather poor description of the system provided by LDA when the number of unpaired spins is large. This fact has already been observed in Fig. 6, which shows that the relative difference between the two approximations has a peak at four electrons in the dot. In other words, the LDA staircase is good enough as long as the spins are mostly paired, otherwise it does not accurately account for the many-body interactions.

We now estimate pairwise electron-electron interaction energies. The so-called s-s interaction between two s electrons can be calculated directly from $E_{\mathrm{xc}}(2)$ and $E_H(2)$ since for two electrons in the dot this is the only possible type of interaction. We have obtained $E_{\mathrm{ee}}^{s\text{-}s}\sim 13$ meV, which is only the Hartree interaction since there is no exchange between the s electrons. Since experiments can only detect average electron-electron interactions, we have only calculated approximate values for the p-s and p-p interactions. The charging energy of the third electron contains one s-s interaction and two p-s interactions. Assuming that the s-s interaction does not change much when the third electron is

TABLE III. Charging energy per electron pair (in meV).

Interaction type	Calculated	Measured (Ref. 5)
s-*s*	13	~ 23
s-*p*	~ 9	~ 7
p-*p*	~ 9	~ 18

added, we have derived the average energy for the p-s interaction to be $E_{ee}^{p-s}\sim 9$ meV. This result is an average because the p electron interacts by exchange with only one of the s electrons (the one with the same spin). Repeating the same argument for the next electrons, we obtained an average p-p interaction of $E_{ee}^{p-p}\sim 9$ meV. Table III summarizes and compares those results with the values inferred from the capacitance data by Fricke *et al.* Differences between energies obtained from calculation and inferred from measurement may result from our assumption that the different types of interaction (s-s, p-s, or p-p) remain unchanged as more electrons are added to the dot. A second source of error in our calculation is the exclusion of interdot repulsion, which should push the electrons closer together inside the dot. However, as we have already pointed out, for dot densities of $10^{10}/\mathrm{cm}^2$, the inclusion of interdot effects should change our results by less than 1 meV. Finally, the approximation used to calculate E_H may lead to some correction in our calculation. As far as the analysis of the experimental data is concerned,[5] it considered the image charge effect but excluded interdot repulsion. In fact, these two competing effects nearly cancel each other for dot densities in the range of $1-10\times 10^{10}/\mathrm{cm}^2$. The analysis of the experimental data also excluded the presence of a charged interface between the gates (the layer of dots charged with one electron each). Indeed, the presence of the layer of charged dots between the gates *decreases* the electron-electron interaction energy by $\sim \gamma_{\mathrm{dot}}\times 3$ meV, where $\rho_{\mathrm{dot}}=\gamma_{\mathrm{dot}}\times 10^{10}/\mathrm{cm}^2$ is the density of dots in the plane. Because this correction is considerably large and linear on γ_{dot}, it is clear that the extraction of the electron-electron energy from the experimental data requires precise knowledge of the dot density.

IV. CONCLUSION

We have calculated the electronic structure of self-assembled InAs-GaAs quantum dots as a function of dot size and externally applied voltage. In order to account for the spin polarization of the system depending on the number of electrons in the dot, we have used LSDA to calculate the electron-electron exchange-correlation energy and compared the results with calculations performed with LDA. We have also used the concept of a transition state[26] to determine the number of electrons in the dot, which minimizes the total energy of the system. We have verified that Hund's rule applies to InAs QD's due to the small charging energy difference of $\sim$ 3 meV between the spin configurations $1s^{\uparrow}1s^{\downarrow}2p_x^{\uparrow}2p_y^{\downarrow}$ and $1s^{\uparrow}1s^{\downarrow}2p_x^{\uparrow}2p_y^{\uparrow}$. We have estimated the charging energy per electron pair, in good agreement with experiment.

ACKNOWLEDGMENTS

We would like to thank Dr. In-Ho Lee, Satyadev Nagaraja, Vivek Rao, and John Shumway for many valuable discussions. One of us (L.F.) acknowledges Yong-Hoon Kim for writing the interface for the LSDA code. This work was supported by CRI from the University of Illinois and NSF Grants No. ECS 95-09751 and No. DMR 94-22496.

APPENDIX A: DERIVATION OF SECOND-ORDER ACCURATE ELECTRON EFFECTIVE MASS

Using perturbation theory up to second-order approximation for the $\mathbf{k}\cdot\mathbf{p}$ Hamiltonian and small values of the wave vector $\mathbf{k}$, we can write the electron effective-mass tensor $m^*_{\alpha\beta}$ as[12]

$$\left(\frac{1}{m^*}\right)_{\alpha\beta}=\frac{1}{m}\delta_{\alpha\beta}+\frac{1}{m^2}\sum_{n'\neq n}\frac{p^{\alpha}_{nn'}p^{\beta}_{n'n}+p^{\beta}_{nn'}p^{\alpha}_{n'n}}{E_n(0)-E_{n'}(0)}, \tag{A1}$$

where m is the bare electron mass and the momentum matrix elements $\mathbf{p}_{nn'}$ are defined as

$$\mathbf{p}_{nn'}=\int_{\text{unit cell}} u^*_{n0}(\mathbf{r})\mathbf{p}u_{n'0}(\mathbf{r})d^3\mathbf{r}, \tag{A2}$$

with the periodic functions $u_{n\mathbf{k}}(\mathbf{r})$ normalized as

$$\int_{\text{unit cell}} u^*_{n\mathbf{k}}(\mathbf{r})u_{n'\mathbf{k}}(\mathbf{r})d^3\mathbf{r}=\delta_{nn'}. \tag{A3}$$

Within the Kane's model for band structure, the near-band-edge basis wave-functions are

$$\begin{aligned}
&\phi_c^{\alpha}=|iS\downarrow\rangle, \quad \phi_{\mathrm{hh}}^{\alpha}=\frac{1}{\sqrt{2}}|-(X+iY)\uparrow\rangle,\\
&\phi_{\mathrm{lh}}^{\alpha}=\frac{1}{\sqrt{6}}|X-iY\uparrow\rangle+\sqrt{\tfrac{2}{3}}|Z\downarrow\rangle,\\
&\phi_c^{\beta}=|iS\uparrow\rangle, \quad \phi_{\mathrm{hh}}^{\beta}=\frac{1}{\sqrt{2}}|X-iY\downarrow\rangle,\\
&\phi_{\mathrm{lh}}^{\beta}=\frac{1}{\sqrt{6}}|-(X+iY)\downarrow\rangle+\sqrt{\tfrac{2}{3}}|Z\uparrow\rangle,
\end{aligned} \tag{A4}$$

where $|Z\rangle$ and $|X\pm iY\rangle$ have the angular symmetry of the spherical harmonics Y_{10} and $Y_{1\pm 1}$, respectively, and the subscripts c, hh, and lh stand for conduction, heavy-hole, and light-hole band, respectively. Here we neglect the splitoff band since it is very weakly coupled to the other bands.

Let us now calculate the electron effective mass in the z direction $m^*_{zz}\equiv m^*_z$, perpendicular to the wetting layer plane. Substituting n by c and n' by lh and hh, Eq. (A1) becomes

$$\left(\frac{1}{m^*}\right)_z=\frac{1}{m}+\frac{2}{m^2}\left(\frac{|p^z_{c,\mathrm{lh}}|^2}{E_c-E_{\mathrm{lh}}}+\frac{|p^z_{c,\mathrm{hh}}|^2}{E_c-E_{\mathrm{hh}}}\right). \tag{A5}$$

Using parity arguments, it is easy to see from Eqs. (A2) and (A4) that $|\mathbf{p}^z_{c,\mathrm{hh}}|=0$. $|\mathbf{p}^z_{c,\mathrm{lh}}|$ can be eliminated from Eq. (A5) using, in the absence of strain, $E_c-E_{\mathrm{lh}}=E_g$ and $m^*_z=m^*$, where E_g is the band-gap energy and m^* is the the bulk electron effective mass. We have assumed that the matrix element $|\mathbf{p}^z_{c,\mathrm{lh}}|$ does not change significantly with or without strain. Therefore, the expression for the electron effective mass in the z direction,

$$m^*_z=m^*\frac{E_c-E_{\mathrm{lh}}}{E_g}, \tag{A6}$$

follows trivially. The only difference between the calculation of m^*_z and the in-plane effective electron masses m^*_x and m^*_y is that both matrix elements $|\mathbf{p}^{x,y}_{c,\mathrm{hh}}|$ and $|\mathbf{p}^{x,y}_{c,\mathrm{lh}}|$ are nonzero, but the calculation steps remain the same.

Comparison with an eight-band $\mathbf{k}\cdot\mathbf{p}$ calculation shows that the procedure above leads to energy levels (from the conduction band edge) approximately $5-10\,\%$ higher than the exact values, while producing enormous savings in computer resources.[15] The description of a more accurate approximation to the eight-band $\mathbf{k}\cdot\mathbf{p}$ theory will be published elsewhere.

*Electronic address: fonseca@ceg.uiuc.edu

[1] S. Fafard, K. Hinzer, S. Raymond, M. Dion, J. McCaffrey, Y. Feng, and S. Charbonneau, Science **274**, 1350 (1996).

[2] J. L. Jimenez, L. R. C. Fonseca, D. E. Wohlert, Y. K. Cheng, D. Brady, and J. P. Leburton, Appl. Phys. Lett. **71**, 3558 (1997).

[3] K. Imamura, Y. Sugiyama, Y. Nakata, S. Muto, and N. Yokoyama, Jpn. J. Appl. Phys., Part 1 **34**, 1445 (1995).

[4] S. Tarucha, D. G Austing, T. Honda, R. J. van der Hage, and L. P. Kouwenhoven, Phys. Rev. Lett. **77**, 3613 (1996).

[5] M. Fricke, A. Lorke, J. P. Kotthaus, G. Medeiros-Ribeiro, and P. M. Petroff, Europhys. Lett. **36**, 197 (1996).

[6] M. A. Cusack, P. R. Briddon, and M. Jaros, Phys. Rev. B **54**, R2300 (1996).

[7] M. Grundmann, O. Stier, and D. Bimberg, Phys. Rev. B **52**, 11 969 (1995).

[8] G. Medeiros-Ribeiro, F. G. Pikus, P. M. Petroff, and A. L. Efros, Phys. Rev. B **55**, 1568 (1997).

[9] A. Wojs and P. Hawrylak, Phys. Rev. B **53**, 10 841 (1996).

[10] N. N. Ledentsov *et al.*, in *Solid-State Electronics* (Elsevier, Great Britain, 1996), Vol. 40, Nos. 1–8, p. 785.

[11] J. P. Perdew and Y. Wang, Phys. Rev. B **45**, 13 244 (1992).

[12] S. L. Chuang, *Physics of Optoelectronic Devices* (Wiley, New York, 1995).

[13] S. M. Sze, *Physics of Semiconductor Devices* (Wiley, New York, 1981).

[14] H. Jiang and J. Singh, in *Proceedings of the Eighth Annual Conference on Modulated Semiconductor Structures, MSS8* (unpublished).

[15] J. Jimenez, L. R. C. Fonseca, and J. P. Leburton (unpublished).

[16] W. L. Briggs, *A Multigrid Tutorial* (SIAM, Philadelphia, 1987).

[17] D. Jovanovic and J. P. Leburton, Phys. Rev. B **49**, 10 841 (1994).

[18] R. G. Parr and W. Yang, *Density-Functional Theory of Atoms and Molecules* (Oxford University Press, New York, 1989).

[19] N. W. Ashcroft and N. D. Mermin, *Solid State Physics* (Saunders College, Philadelphia, 1976).

[20] D. M. Ceperley and B. J. Alder, Phys. Rev. Lett. **45**, 566 (1980).

[21] J. P. Perdew and A. Zunger, Phys. Rev. B **23**, 5048 (1981).

[22] O. Gunnarsson and B. I. Lundqvist, Phys. Rev. B **13**, 4274 (1976).

[23] Hund's rule is expected to manifest in quantum dots displaying geometrical symmetries. In that case unpaired spins should occur also for an even number of electrons in the dot.

[24] J. Shumway, L. R. C. Fonseca, J. P. Leburton, Richard M. Martin, and D. Ceperley (unpublished).

[25] M. Stopa, Phys. Rev. B **54**, 13 767 (1996).

[26] J. C. Slater, Adv. Quantum Chem. **6**, 1 (1972).

[27] M. Macucci, K. Hess, and G. J. Iafrate, Phys. Rev. B **48**, 17 354 (1993).

[28] J. F. Janak, Phys. Rev. B **18**, 7165 (1978).

[29] P. H. Dederichs, S. Blugel, R. Zeller, and H. Akai, Phys. Rev. Lett. **53**, 2512 (1984).

[30] M. S. Hybertsen, M. Schluter, and N. E. Christensen, Phys. Rev. B **39**, 9028 (1989).

[31] T. Inui, Y. Tarabe, and Y. Onodera, *Group Theory and its Applications in Physics* (Springer, New York, 1996).

[32] R. J. Luyken, A. Lorke, M. Haslinger, B. T. Miller, M. Fricke, J. P. Kotthaus, G. Medeiros-Ribeiro, and P. M. Petroff (unpublished).